Vietnam Journal of Mechanics, Vol. 47, No. 4 (2025), pp. 381 – 396
DOI: https://doi.org/10.15625/0866-7136/23362

MULTIPHASE TOPOLOGY OPTIMIZATION FOR THE DESIGN OF POROUS METAMATERIALS WITH LOCAL VOLUME CONSTRAINT

Minh Ngoc Nguyen[1,2*], **Chanh Dinh Vuong**[1,2], **Hung Thanh Tran**[1,2], **Tinh Quoc Bui**[1,2]
[1]*Duy Tan Research Institute for Computational Engineering (DTRICE), Duy Tan University, Ho Chi Minh City 70000, Vietnam*
[2]*Faculty of Civil Engineering, Duy Tan University, Da Nang 50000, Vietnam*
[*]E-mail: nguyenngocminh6@duytan.edu.vn

Received: 16 September 2025 / Revised: 29 September 2025 / Accepted: 30 November 2025
Published online: 04 December 2025

Abstract. This paper presents a novel multiphase approach for topological design of porous metamaterials. Firstly, a new interpolation scheme based on partition-of-unity mapping is proposed. The scheme is employed into the design of periodic metamaterials with specified expectation on effective properties. Due to the periodicity, the design domain is defined in a Representative Unit Cell (RUC) - which represents the repeated pattern - such that the effective (or homogenized) elastic tensor is evaluated by the Strain Energy Method (SEM). In order to reduce the computational effort, the pattern is assumed to be symmetric, which is equivalent to finding metamaterials with orthotropic behavior. The allowed amount of each material is given via upper bound constraints on global volume fraction. The pore size is further controlled by requiring local volume constraint on each material phase. Via several numerical examples, which differ from each other in terms of objective function and the amount of each material phase, the feasibility of the proposed approach is demonstrated.

Keywords: partition-of-unity mapping, multi-material topology optimization, periodic metamaterials, local volume constraint.

1. INTRODUCTION

Artificial metamaterials have gained increasing attention during the last decades, as they can be designed to exhibit interesting properties, some of which may even be

rarely observed in natural materials, e.g., the negative Poisson's ratio in auxetic structures. A metamaterial is composed of periodic arrangement of microstructures (or Representative Unit Cell - RUC). The effective property of a metamaterial depends not only on the base materials but also on the shape of microstructures as well as the way the microstructures are arranged. In the context of designing metamaterials by topology optimization, the objective is finding the topological shape that maximizes/minimizes a specified property, e.g., maximization of bulk modulus or shear modulus, or minimization of Poisson's ratio. Some basic aspects on using numerical homogenization to determine the effective property of periodic microstructures were discussed by Andreassen and Andreasen [1]. Later, Xia and Breitkopf [2] presented a Matlab code for design of metamaterials by topology optimization, on the basis of energy-based homogenization. Alternatively, the effective elastic tensor of a RUC can be evaluated via the strain energy method (SEM) [3]. Although with this method, the searching space is limited to symmetric orthotropic micro-structures, fast computation can be expected. Design of single-material microstructures with consideration of stress constraint was discussed by Collet et al. [4] and later by Gupta et al. [5] with more focus on auxetic metamaterials. Various multi-material schemes for design of microstructure with multiple base materials were also proposed in the literature [6–8].

The idea of local volume constraint was originally presented by Wu et al. [9], in an attempt to generate bone-like porous structures. Some expected benefits include generation of lightweight yet stable structures which are suitable for additive manufacturing. Further elaboration was conducted by various authors. Fernandez et al. [10] utilized the concept to control maximum size. Das and Sutradhar [11] introduced a technique to design functionally graded porous structures based on local volume constraint. Wang et al. [12] employed the local volume constraint for design of infill structures with consideration of the material's allowable stress. Zhou et al. [13] proposed a concurrent approach for shell-infill structure in which the outer shell (coating) is obtained based on usual topology optimization with global volume constraint, while the infill is generated via topology optimization with local volume constraint. Postigo et al. [14] extended the shell-infill design one more step forward by taking the coating thickness into account, on the basis of the so-called SUSAN algorithm.

To the best of the authors' knowledge, the design of metamaterials with local volume constraint has not been discussed in the available literature. In fact, an experimental study by Han et al. [15] has mentioned that under uniaxial compression test, it is not necessary to keep large solid region in the auxetic structure because stress field tends to concentrate in certain area while its value is low in other area. Therefore, they recommended a frame-like structure with stiffened ribs (to ensure stability), which also reduces the size

of holes. It was reported that their proposed structure even has higher specific energy absorption than the usual counterpart. Being inspired by the work by Han et al. [15], in this paper, the local volume constraint is incorporated into the design of periodic metamaterials by topology optimization, resulting in new layouts that have not been presented in the literature. Furthermore, a novel partition-based mapping scheme is developed for multiphase meta-materials. Unlike the existing p-norm mapping scheme [16], the proposed scheme explicitly enforces the requirement on partition-of-unity property for the design variables, i.e., the sum of volume fraction of all material phases (including the voided phase) within every element must be exactly one. This requirement removes the spurious case mentioned in [16], where the design variables in an arbitrary element could all be one, meaning that the total volume of the materials filled in the element of interest is even larger than the volume of the element itself.

The rest of the paper is organized as follows. Immediately after the Introduction, the key points of the novel partition-of-unity mapping (PUM) scheme for multi-material topology optimization are presented in Section **2.1**. In Section **2.2**, the PUM scheme is employed to formulate the design of multiphase porous metamaterials with local volume constraints. The feasibility of the proposed method is demonstrated in Section **3**, where several types of periodic metamaterials are investigated. Finally, some concluding remarks are given in Section **4**.

2. FORMULATION

2.1. Partition-of-unity mapping for multi-material topology optimization

The idea of using a separate set of design variables to represent each solid material was recently presented by Yi et al. [16]. That is, in every element, M design variables (in the range from 0 to 1) corresponding to M solid materials are defined at the element centroid. The usual three-field density approach (i.e., original field, filtered field, and projected field) is firstly applied to each set of variables. The projected values (of all sets) are passed into p-norm-based mapping functions. Finally, material properties are interpolated from the mapped values in a manner similar to the Solid Isotropic Material with Penalization - SIMP (see more details in Refs. [16–18]). The p-norm mapping approach has many advantages: (i) each set of design variables directly represents one material phase (instead of using a certain combination of variables to represent one material phase like in the extended version of SIMP for multiple materials); and (ii) the formulation can be straightforwardly generalized to arbitrary number of materials.

However, the p-norm mapping scheme has an inherent drawback. Design variables are defined only for solid materials, and the projected values (of the design variables) are interpreted as the physical densities of solid materials (i.e., the volume fraction of the

materials within an element). Therefore, an element is inferred to be left voided if all the design variables (associated with that element) are zero. On the other hand, the case where all the design variables are equal to one is theoretically possible. This spurious case was not treated in [16].

Here, we propose a new partition-of-unity mapping (PUM) concept as follows:

- The number of design variables in each element is equal to the number of material phases involved (including the voided phase).

- Partition-of-unity property is explicitly enforced, i.e., the sum of design variables in every element must be exactly one.

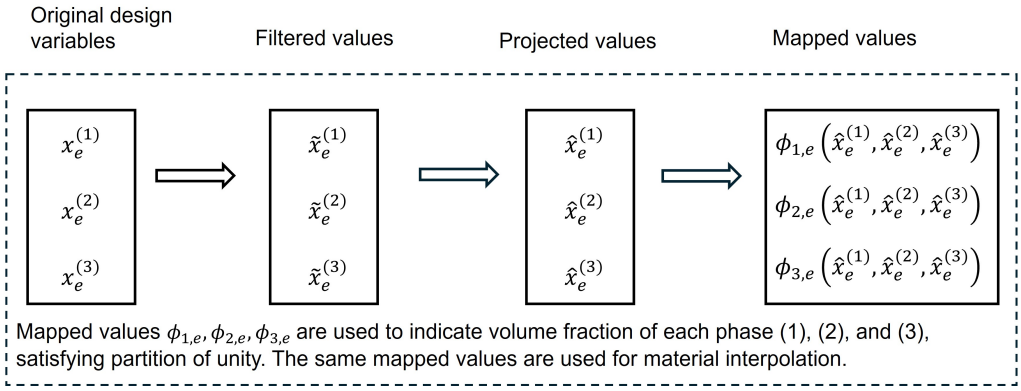

Fig. 1. Illustrative sketch of the PUM concept for 3-phase problems (e.g., 2 solid materials and 1 voided phase)

Without loss of generality, a 3-phase example is taken to demonstrate the proposed scheme (see Fig. 1 for illustration). Since there are three phases, three design variables are designated in each element, namely $x_e^{(1)}, x_e^{(2)}, x_e^{(3)}$. Filter and projection are applied to each set of variables (i) as follows

$$\text{Filter:} \qquad \tilde{x}_e^{(i)} = \frac{1}{\sum\limits_{k\in S_e} w_{ek}} \sum_{j\in S_e} x_j^{(i)} w_{ej}, \tag{1}$$

$$\text{Projection:} \quad \hat{x}_e^{(i)} = \frac{\tanh(\frac{1}{2}\beta) + \tanh(\beta(\tilde{x}_e^{(i)} - \frac{1}{2}))}{2\tanh(\frac{1}{2}\beta)}. \tag{2}$$

In Eq. (1), the filtered value is computed as a weighted average, where the weight w_{ej} decreases based on the distance Δ_{ej} between the centroids of element e and element j. For simplicity, a circular region originated at the centroid of the element of interest e is defined with radius $r_{\min}$. S_e denotes the collection of elements k whose centroids are

located within the circular region. The weight is then determined by

$$w_{ej} = \max\left(0, \frac{r_{\min} - \Delta_{ej}}{r_{\min}}\right). \tag{3}$$

The role of projection in Eq. (2) is to boost the clarity in the topological results, i.e., variables larger than 0.5 will be pushed to 1, otherwise they will be pushed to 0. For numerical stability, the parameter β is usually taken as 1 in the beginning, and is gradually increased during the optimization process. The key point of the proposed method is the explicit requirement on the partition of unity of the material volume fraction. Neither the original variables, the filtered variables, nor the projected variables possess the property. Therefore, the partition of unity is enforced by constructing the mapping functions in rational form

$$\phi_{1,e}\left(\hat{x}_e^{(1)}, \hat{x}_e^{(2)}, \hat{x}_e^{(3)}\right) = \frac{\hat{x}_e^{(1)}}{\hat{x}_e^{(1)} + \hat{x}_e^{(2)} + \hat{x}_e^{(3)}}, \tag{4}$$

$$\phi_{2,e}\left(\hat{x}_e^{(1)}, \hat{x}_e^{(2)}, \hat{x}_e^{(3)}\right) = \frac{\hat{x}_e^{(2)}}{\hat{x}_e^{(1)} + \hat{x}_e^{(2)} + \hat{x}_e^{(3)}}, \tag{5}$$

$$\phi_{3,e}\left(\hat{x}_e^{(1)}, \hat{x}_e^{(2)}, \hat{x}_e^{(3)}\right) = \frac{\hat{x}_e^{(3)}}{\hat{x}_e^{(1)} + \hat{x}_e^{(2)} + \hat{x}_e^{(3)}}. \tag{6}$$

It is obvious that the sum of mapped values is exactly one. Hence, they are used to indicate the volume fraction of the materials. Similar to SIMP method, the elastic modulus is here interpolated by power law as

$$E_e = E^{(1)}\phi_{1,e}^q + E^{(2)}\phi_{2,e}^q + E^{(3)}\phi_{3,e}^q = \sum_i E^{(i)}\phi_{i,e}^q, \tag{7}$$

where $E^{(i)}$ denotes the elastic modulus of material (i). Typically, $q = 3$ is taken. For voided phase, a small positive value is assigned to avoid zero stiffness (in this paper, $E_{void} = 10^{-9}$ is chosen). The volume of material phase (i) is computed by

$$V^{(i)} = \sum_{e=1}^{NE} \phi_i\left(\hat{x}_e^{(1)}, \hat{x}_e^{(2)}, \hat{x}_e^{(3)}\right) V_e, \tag{8}$$

where NE is the number of elements, and V_e is the volume (or area for 2D cases) of element e.

2.2. Design of multiphase porous metamaterials with local volume constraints

The objective in the design of metamaterials is to minimize/maximize an effective property, e.g., maximizing bulk or shear modulus, or minimizing Poisson's ratio. Hence, it is important to accurately evaluate the effective (or homogenized) elastic tensor of the meta-materials, which can be conducted by homogenization method [2,18] or the strain

energy method [3]. Here, we focus on periodic meta-materials, thus the design domain is limited to the Representative Unit Cell (RUC). In the literature, a square domain $L \times L$ is typically defined for the RUC.

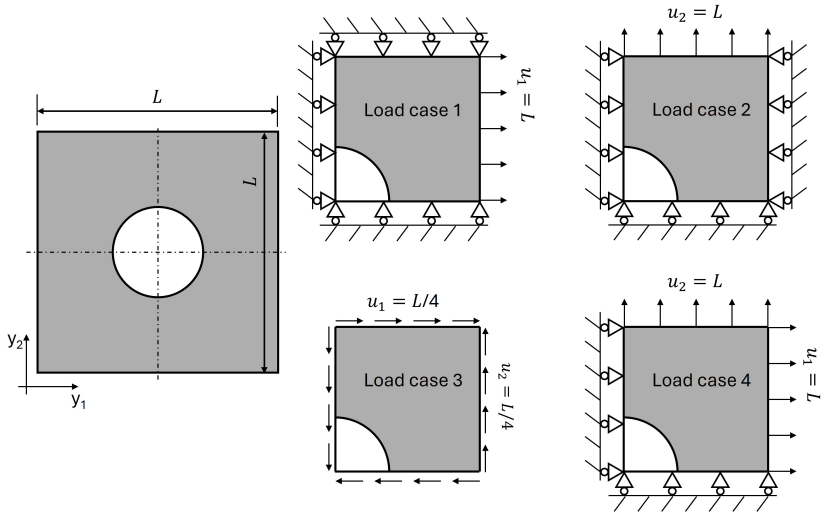

Fig. 2. Quarter model of unit cell (due to symmetry) and boundary conditions for four load cases

With small deformation and linear elastic behavior, the relation between the effective stress tensor $\bar{\sigma}_{ij} = [\bar{\sigma}_{11}, \bar{\sigma}_{22}, \bar{\sigma}_{12}]^T$ and the effective strain tensor $\bar{\varepsilon}_{kl} = [\bar{\varepsilon}_{11}, \bar{\varepsilon}_{22}, 2\bar{\varepsilon}_{12}]^T$ is given by Hooke's law as follows

$$\begin{bmatrix} \bar{\sigma}_{11} \\ \bar{\sigma}_{22} \\ \bar{\sigma}_{12} \end{bmatrix} = \begin{bmatrix} D^H_{1111} & D^H_{1122} & 0 \\ D^H_{2211} & D^H_{2222} & 0 \\ 0 & 0 & D^H_{1212} \end{bmatrix} \begin{bmatrix} \bar{\varepsilon}_{11} \\ \bar{\varepsilon}_{22} \\ 2\bar{\varepsilon}_{12} \end{bmatrix}, \tag{9}$$

where D^H_{ijkl} is the effective (homogenized) elastic tensor. Note that in Eq. (9), the design space has been assumed to be symmetric with respect to both vertical and horizontal directions [3]. Since the elastic tensor is symmetric, i.e., $D^H_{1122} = D^H_{2211}$, there are only four components to be determined. Using the strain energy method (SEM) [3], the four components are computed via four load cases (see Fig. 2): (1) prescribed unit strain along horizontal direction, (2) prescribed unit strain along vertical direction, (3) prescribed shear strain, and (4) prescribed unit strain along both horizontal and vertical directions. The four components of the effective elastic tensor are thus obtained by

$$D^H_{1111} = 2\bar{W}^{(1)},\ D^H_{2222} = 2\bar{W}^{(2)},\ D^H_{1212} = 2\bar{W}^{(3)}, D^H_{1122} = D^H_{2211} = \bar{W}^{(4)} - \bar{W}^{(1)} - \bar{W}^{(2)}, \tag{10}$$

in which $\bar{W}^{(m)}$ denotes the strain energy corresponding to load case (m). Curious readers are referred to Ref. [3] for comparison between the SEM and energy-based homogenization. Using finite element method, the strain energy is computed as follows (the

superscript (m) is dropped here for brevity)

$$\bar{W} = \frac{1}{2}\sum_{e=1}^{NE} \mathbf{U}_e^T \mathbf{K}_e \mathbf{U}_e, \tag{11}$$

where $\mathbf{U}_e$ is the vector of nodal displacements associated with element e; and $\mathbf{K}_e$ is the element stiffness matrix. In every element e, the stiffness matrix is computed using the interpolated elastic modulus given in Eq. (7). In practice, an equilibrium is solved for each of the four load cases as in Fig. 2 to get the four values of strain energy $\bar{W}^{(m)}$. For load case 1, in order to achieve unit strain along horizontal direction, the horizontal displacement of the right edge is prescribed by $u_1 = L$ (L is the side of the square domain), while the vertical displacement of the top edge is restrained. Note that the symmetric conditions have been applied in Fig. 2, as 1/4 of the domain is considered, and $u_1 = 0$ is applied on the left side and $u_2 = 0$ is applied on the bottom side. Load case 2 is similar to load case 1, but now a vertical displacement $u_2 = L$ is applied on the top edge, while the horizontal displacement of the right edge is restrained. In load case 4, $u_1 = L$ is applied on the right edge and $u_2 = L$ is applied on the vertical edge. In load case 3, to simulate the pure shear, Dirichlet boundary conditions are enforced as follows: vertical displacement $u_2 = L/4$ is applied on the right edge, u_1 = L/4 is applied on the top edge, $u_2 = -L/4$ is applied on the left side, and $u_1 = -L/4$ is applied on the bottom side.

The limit on amount of materials is given by the (global) constraint on volume fraction of each material as

$$v^{(i)} \equiv \frac{V^{(i)}}{\sum_{e}^{NE} V_e} \leq \bar{v}^{(i)}, \quad i = 1, 2, 3, \ldots, M, \tag{12}$$

in which $v^{(i)}$ denotes the volume fraction of material phase (i) and $\bar{v}^{(i)}$ is the required upper bound. Note that only M constraints are needed for $(M+1)$-phase problem. If the sum of the volume fraction of solid phases is less than 1, which is common in practice, the obtained metamaterial is porous. Here, we further require local volume constraint, i.e., the volume of solid material within a local domain M_e surrounding an arbitrary element e should not exceed a given value. The local domain M_e is defined in a manner similar to the filter domain S_e in Eq. (1), but with a different radius. Hence, the average volume fraction of material phase (i) within domain M_e is given by

$$\bar{v}_{e,loc}^{(i)} = \frac{1}{\sum_{k \in M_e} V_k} \sum_{j \in M_e} \phi_{j,e}^{(i)} V_j. \tag{13}$$

Direct enforcement of local volume constraint for each domain M_e will lead to NE constraints for each material phase (i). In order to reduce the complexity, the constraint

is reformulated as the maximum value of $\bar{v}_{e,loc}^{(i)}$ should not exceed a predefined value $\alpha^{(i)}$

$$\bar{v}_{e,loc}^{(i)} \leq \max \bar{v}_{e,loc}^{(i)} \leq \alpha^{(i)}. \tag{14}$$

The non-differentiable max function is further approximated by p-norm function to facilitate sensitivity calculation as

$$\max \bar{v}_{e,loc}^{(i)} = c^{(i)} \left(\sum_{e=1}^{NE} \left(\bar{v}_{e,loc}^{(i)} \right)^p \right)^{1/p} \equiv c^{(i)} \bar{v}_{PN,loc}^{(i)}. \tag{15}$$

Theoretically, the p-norm value will tend to the maximum value when the power factor p tends to infinity. Nevertheless, a finite value of p is used in practice. Therefore, the coefficient $c^{(i)}$ is introduced to fill the gap, which is updated in every iteration of optimization process as [19,20]

$$c_{iter+1}^{(i)} = \frac{1}{2} \left(\frac{\max \left(\bar{v}_{e,loc}^{(i)} \right)_{iter+1}}{\left(\bar{v}_{PN,loc}^{(i)} \right)_{iter+1}} \right) + \frac{1}{2} c_{iter}^{(i)}. \tag{16}$$

Initially, $c_0^{(i)} = 1$ is taken.

3. NUMERICAL EXAMPLES

Without loss of generality, the RUC is defined in a unit square domain ($L = 1$). Two artificial materials, namely Red and Blue, are considered, with elastic moduli being $E^{(1)} \equiv E^{(Red)} = 2$ and $E^{(2)} \equiv E^{(Blue)} = 1$. The Poisson's ratio $\nu = 0.3$ is assumed for all materials. Initially, the design variables for both solid materials are set as 0.5 (i.e., $x^{(1)} = x^{(2)} = 0.5$ and $x^{(3)} = 0$), except that a circular region with radius $1/6$ originated at the center is left voided (i.e., $x^{(1)} = x^{(2)} = 0$ and $x^{(3)} = 1$). Due to symmetry, a quarter domain is modeled with a uniform discretization of 100×100 four-node quadrilateral elements. The power factor $q = 3$ is taken for material interpolation (see Eq. (7)), while $p = 16$ is used for the p-norm approximation (Eq. (15)). The radius $r_{\min}$ for density filter is 4 element lengths, and that for local volume constraint is 10 element lengths. Parameter β in the projection (Eq. (2)) is set as 1 in the beginning. For every 20 iterations, β is increased by 1, until the maximum value $\beta_{\max} = 32$ is reached. The design variables are updated by the Method of Moving Asymptotes (MMA) [21], with the so-called "move limit" (a parameter in MMA) being set as 0.1. The optimization is considered as converged when all the following conditions are simultaneously achieved: (i) the continuation scheme is complete (i.e., $\beta = \beta_{\max}$), (ii) both the global and local volume constraints are satisfied, and (iii) the maximum difference between the design variables of the current iteration and the previous one is less than 0.01.

Three types of objective function are studied as follows [2,4]:

For maximizing bulk modulus: $$f_{obj} = -\left(D^H_{1111} + D^H_{2222} + D^H_{1122} + D^H_{2211}\right) \quad (17)$$

For maximizing shear modulus: $$f_{obj} = -\left(D^H_{1212}\right) \quad (18)$$

For minimizing Poisson's ratio: $$f_{obj} = D^H_{1122} - 0.1\left(D^H_{1111} + D^H_{2222}\right) \quad (19)$$

For each type, two cases of global volume constraint and two cases of local volume constraint are considered:

- Global volume constraint: (1) 30% Red and 20% Blue, (2) 20% Red and 30% Blue.

- Local volume constraint: (a) $\alpha^{(Red)} = \alpha^{(Blue)} = 0.5$, (b) $\alpha^{(Red)} = 0.4$ and $\alpha^{(Blue)} = 0.6$.

Since both global and local volume constraints are required in the design, there are six cases in total for each type of objective function: Case 1, Case 2, Case 1a, Case 1b, Case 2a and Case 2b.

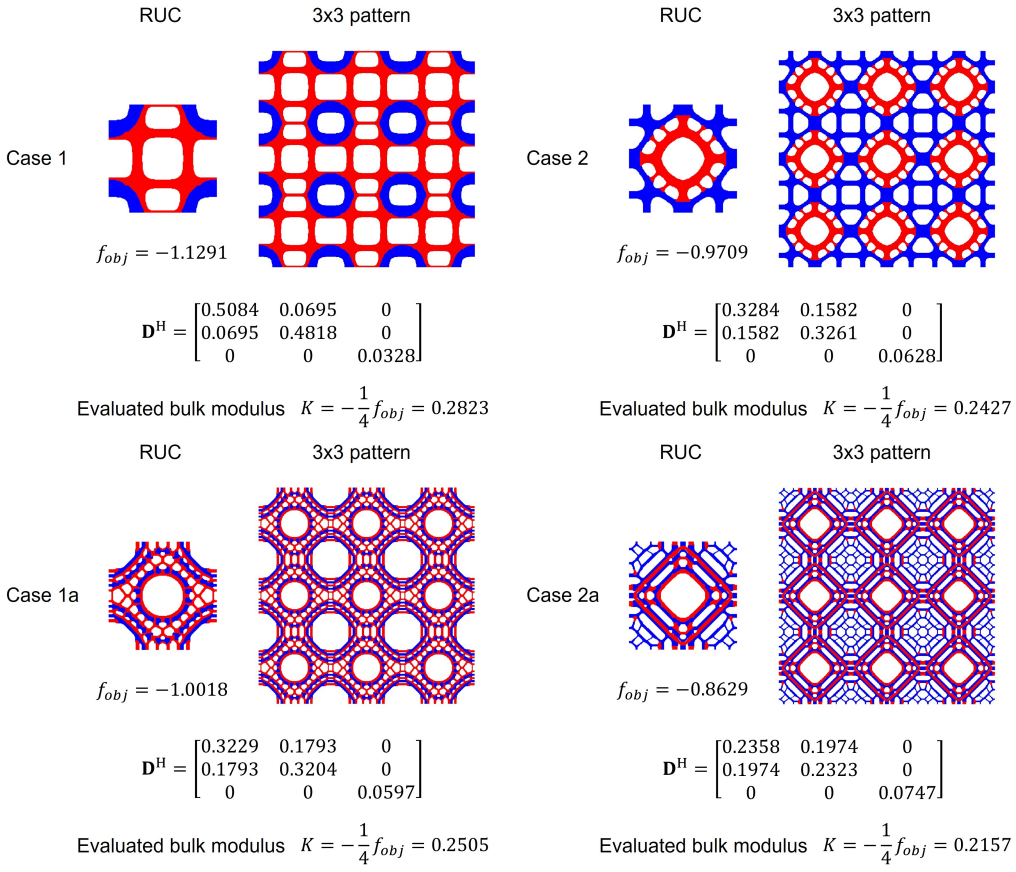

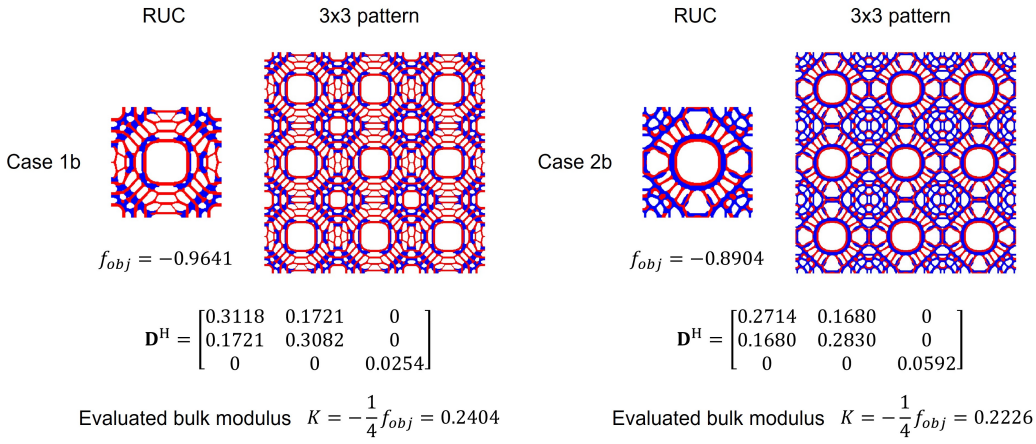

Fig. 3. Three-phase designs for maximized bulk modulus

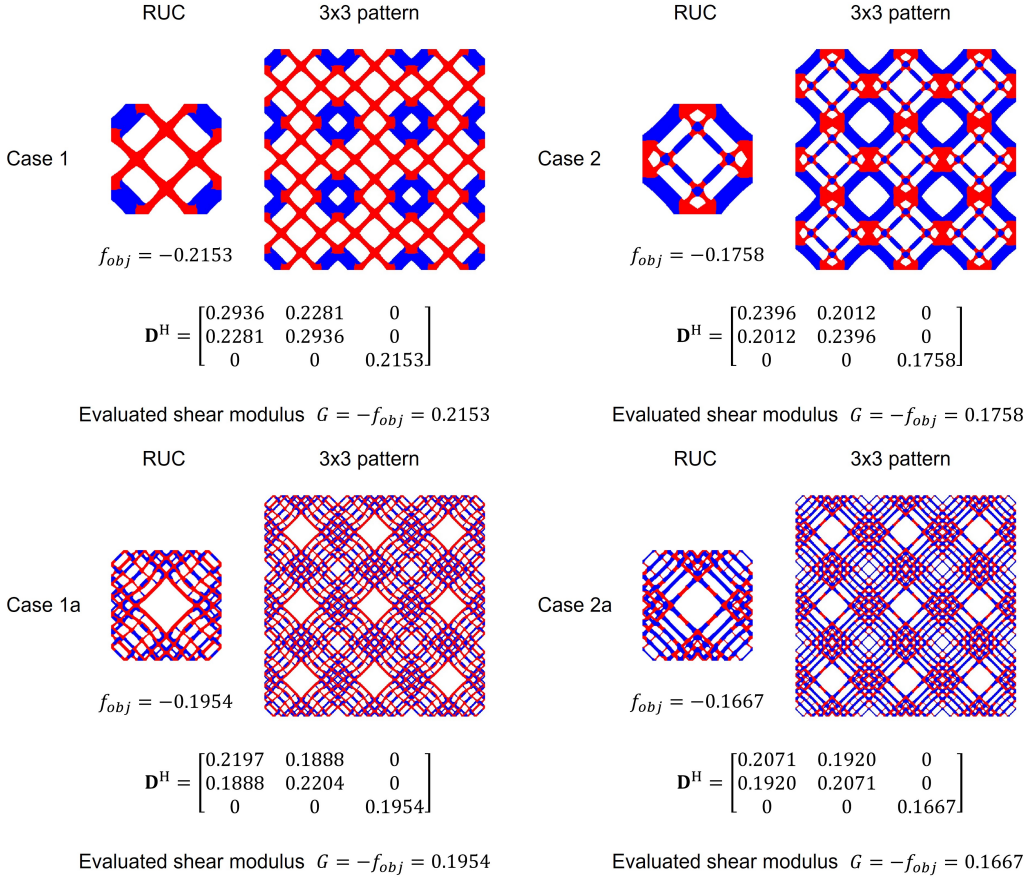

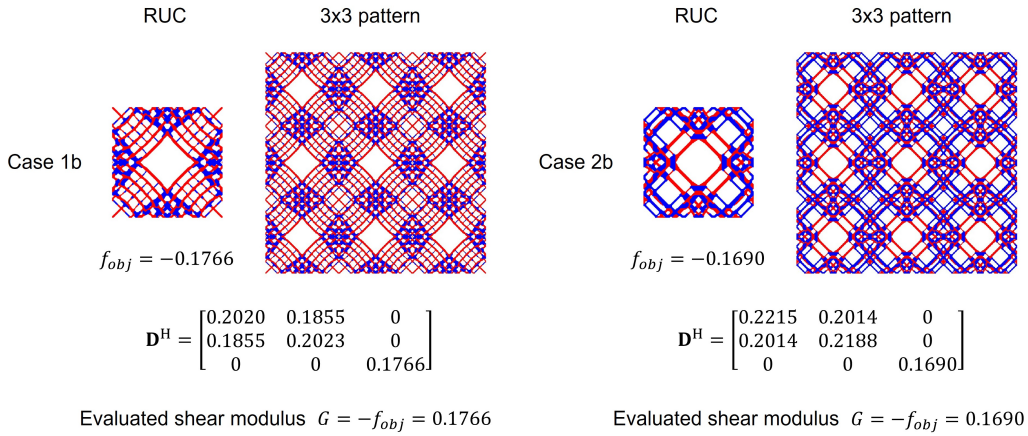

Fig. 4. Three-phase designs for maximized shear modulus

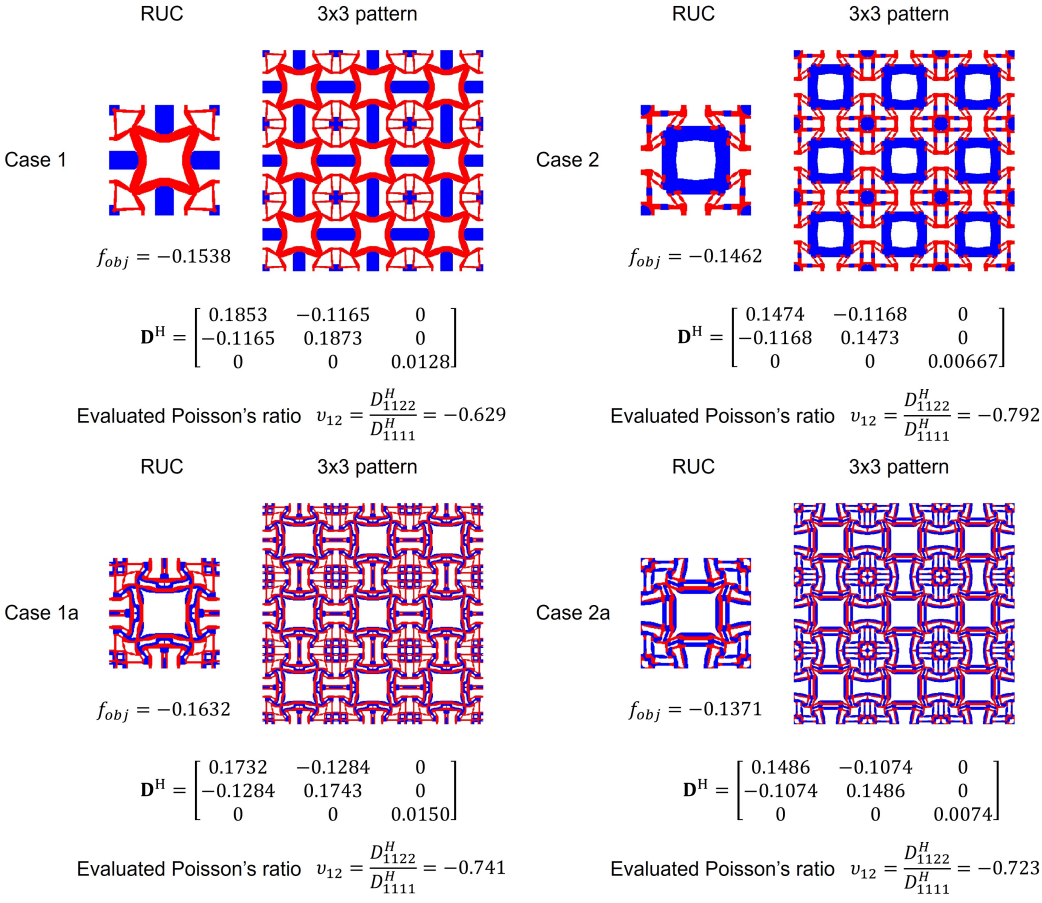

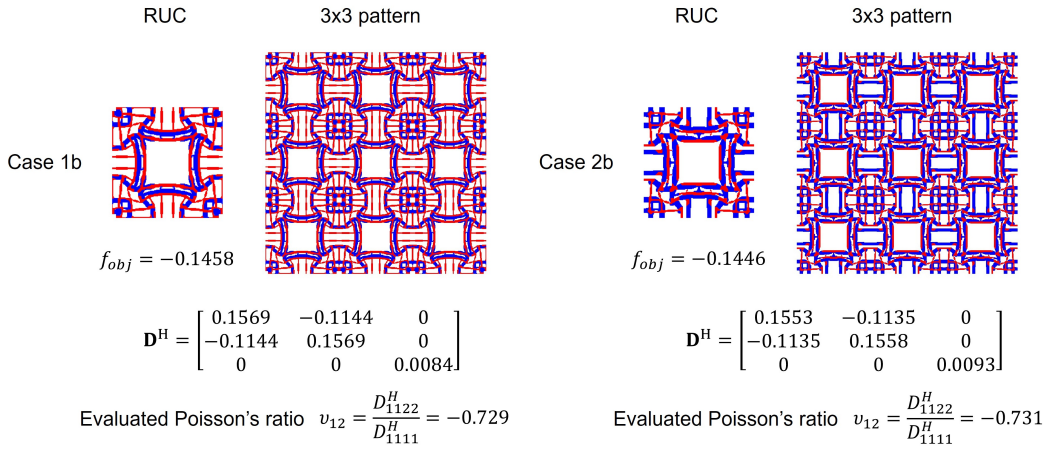

Fig. 5. Three-phase designs for minimized Poisson's ratio

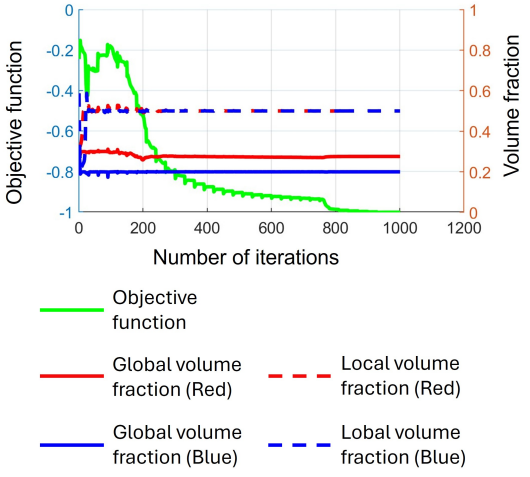

Fig. 6. History curves for Case 1a of maximized bulk modulus

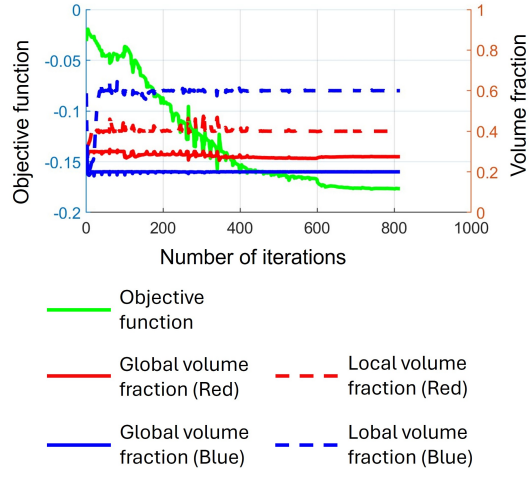

Fig. 7. History curves for Case 1b of maximized shear modulus

Fig. 3 presents the designs for maximized bulk modulus. It is seen that without consideration of local volume constraints, thick features are formed for both materials Red and Blue. When local volume constraints are involved, as expected, material tends to be spread in the design domain, creating more thin features. The same observation is recorded in the designs for maximized shear modulus (Fig. 4) and minimized Poisson's ratio (Fig. 5). In Fig. 5, the designs even exhibit negative Poisson's ratio. It is demonstrated via the numerical examples that it is possible to enforce different requirements on local volume of each material phase. This finding is important, as it is preliminary for further development on techniques to control the pore size at the design stage. For

each type of objective function, the history curves for one case of volume constraints are presented, see Fig. 6 for Case 1a of maximized bulk modulus, Fig. 7 for Case 1b of maximized shear modulus, and Fig. 8 for Case 2b of minimized Poisson's ratio. All the history curves exhibit that convergence has been achieved for the objective function, and the volume constraints (either global volume or local volume) are satisfied.

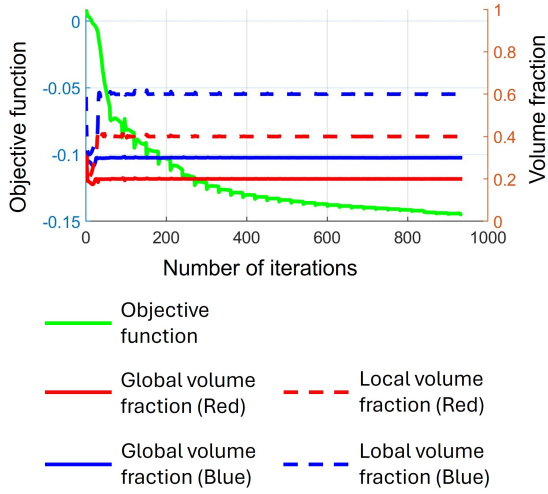

Fig. 8. History curves for Case 2b of minimized Poisson's ratio

4. CONCLUSION

A new approach for multi-material topology optimization based on partition-of-unity mapping is introduced and employed in the design of periodic meta-materials. The current scheme inherits desirable features of the existing p-norm mapping scheme [16], such as simplicity and straightforward generalization. The distinctive differences are: (i) the mapped values of the design variables are used in both calculation of volume fraction (of each material phase) and calculation of material stiffness, and (ii) the partition-of-unity property is explicitly enforced.

Furthermore, the concept of local volume constraint is introduced into the design of multiphase meta-materials. Due to the requirement on local volume fraction, materials are distributed such that both large solid regions and large voided regions are reduced. Considering that metamaterials are porous, the obtained results are preliminary for further research on techniques to control the pore size of periodic metamaterials at the RUC level. A limit on minimum length scale for the thin features is therefore necessary. Also, the existence of thin features leads to the need to control the stress concentration and possible buckling in the structure. These aspects are interesting topics for future work.

The assumption of symmetry in SEM (see Section **2.1**) indeed narrows the design space to an orthotropic unit cell. On the other hand, the symmetric condition allows the modeling of a quarter domain, significantly reducing computational cost. Nevertheless, the concept proposed in this paper can be conducted by using other homogenization techniques, with or without the symmetric/orthotropic assumption.

Regarding the implementation aspect, curious readers are referred to Ref. [2] for a Matlab code tailored to topological design of porous meta-materials, using energy-based homogenization. The given code could be converted to the strain energy method without much difficulty. For local volume constraint, a good reference is Ref. [9], where an algorithm box with pseudo-code is provided.

DECLARATION OF COMPETING INTEREST

The authors declare that they have no known competing financial interests or personal relationships that could have appeared to influence the work reported in this paper.

ACKNOWLEDGMENT

This research is funded by Vietnam National Foundation for Science and Technology Development (NAFOSTED) under grant number 107.02-2023.100. We acknowledge the support of time and facilities from Duy Tan University for this study.

REFERENCES

[1] E. Andreassen and C. S. Andreasen. How to determine composite material properties using numerical homogenization. *Computational Materials Science*, **83**, (2014), pp. 488–495. https://doi.org/10.1016/j.commatsci.2013.09.006.

[2] L. Xia and P. Breitkopf. Design of materials using topology optimization and energy-based homogenization approach in Matlab. *Structural and Multidisciplinary Optimization*, **52**, (2015), pp. 1229–1241. https://doi.org/10.1007/s00158-015-1294-0.

[3] W. Zhang, G. Dai, F. Wang, S. Sun, and H. Bassir. Using strain energy-based prediction of effective elastic properties in topology optimization of material microstructures. *Acta Mechanica Sinica*, **23**, (2007), pp. 77–89. https://doi.org/10.1007/s10409-006-0045-2.

[4] M. Collet, L. Noël, M. Bruggi, and P. Duysinx. Topology optimization for microstructural design under stress constraints. *Structural and Multidisciplinary Optimization*, **58**, (2018), pp. 2677–2695. https://doi.org/10.1007/s00158-018-2045-9.

[5] A. Gupta, A. Gupta, and R. Chowdhury. Computational design of auxetic microstructures via stress-based topology optimization. *Engineering Structures*, **319**, (2024). https://doi.org/10.1016/j.engstruct.2024.118807.

[6] Y. Wang, J. Gao, Z. Luo, T. Brown, and N. Zhang. Level-set topology optimization for multimaterial and multifunctional mechanical metamaterials. *Engineering Optimization*, **49**, (2016), pp. 22–42. https://doi.org/10.1080/0305215x.2016.1164853.

[7] P. Vogiatzis, S. Chen, X. Wang, T. Li, and L. Wang. Topology optimization of multi-material negative Poisson's ratio metamaterials using a reconciled level set method. *Computer-Aided Design*, **83**, (2017), pp. 15–32. https://doi.org/10.1016/j.cad.2016.09.009.

[8] Z. Han and K. Wei. Multi-material topology optimization and additive manufacturing for metamaterials incorporating double negative indexes of Poisson's ratio and thermal expansion. *Additive Manufacturing*, **54**, (2022). https://doi.org/10.1016/j.addma.2022.102742.

[9] J. Wu, N. Aage, R. Westermann, and O. Sigmund. Infill optimization for additive manufacturing—approaching bone-like porous structures. *IEEE Transactions on Visualization and Computer Graphics*, **24**, (2018), pp. 1127–1140. https://doi.org/10.1109/tvcg.2017.2655523.

[10] E. Fernández, M. Collet, P. Alarcón, S. Bauduin, and P. Duysinx. An aggregation strategy of maximum size constraints in density-based topology optimization. *Structural and Multidisciplinary Optimization*, **60**, (2019), pp. 2113–2130. https://doi.org/10.1007/s00158-019-02313-8.

[11] S. Das and A. Sutradhar. Multi-physics topology optimization of functionally graded controllable porous structures: Application to heat dissipating problems. *Materials & Design*, **193**, (2020). https://doi.org/10.1016/j.matdes.2020.108775.

[12] J. Wang, J. Wu, and R. Westermann. Stress topology analysis for porous infill optimization. *Structural and Multidisciplinary Optimization*, **65**, (2022). https://doi.org/10.1007/s00158-022-03186-0.

[13] M. Zhou, Y. Lu, Y. Liu, and Z. Lin. Concurrent topology optimization of shells with self-supporting infills for additive manufacturing. *Computer Methods in Applied Mechanics and Engineering*, **390**, (2022). https://doi.org/10.1016/j.cma.2021.114430.

[14] J. A. Postigo, A. Garaigordobil, R. Ansola, and J. Canales. Topology optimization of Shell–Infill structures with enhanced edge-detection and coating thickness control. *Advances in Engineering Software*, **189**, (2024). https://doi.org/10.1016/j.advengsoft.2023.103587.

[15] D. Han, X. Ren, Y. Zhang, X. Yu Zhang, X. Gang Zhang, C. Luo, and Y. Min Xie. Lightweight auxetic metamaterials: Design and characteristic study. *Composite Structures*, **293**, (2022). https://doi.org/10.1016/j.compstruct.2022.115706.

[16] B. Yi, G. H. Yoon, R. Zheng, L. Liu, D. Li, and X. Peng. A unified material interpolation for topology optimization of multi-materials. *Computers & Structures*, **282**, (2023). https://doi.org/10.1016/j.compstruc.2023.107041.

[17] O. Sigmund. A 99 line topology optimization code written in Matlab. *Structural and Multidisciplinary Optimization*, **21**, (2001), pp. 120–127. https://doi.org/10.1007/s001580050176.

[18] E. Andreassen, A. Clausen, M. Schevenels, B. S. Lazarov, and O. Sigmund. Efficient topology optimization in MATLAB using 88 lines of code. *Structural and Multidisciplinary Optimization*, **43**, (2010), pp. 1–16. https://doi.org/10.1007/s00158-010-0594-7.

[19] H. Liu, D. Yang, P. Hao, and X. Zhu. Isogeometric analysis based topology optimization design with global stress constraint. *Computer Methods in Applied Mechanics and Engineering*, **342**, (2018), pp. 625–652. https://doi.org/10.1016/j.cma.2018.08.013.

[20] S. Xu, J. Liu, B. Zou, Q. Li, and Y. Ma. Stress constrained multi-material topology optimization with the ordered SIMP method. *Computer Methods in Applied Mechanics and Engineering*, **373**, (2021). https://doi.org/10.1016/j.cma.2020.113453.

[21] K. Svanberg. The method of moving asymptotes—a new method for structural optimization. *International Journal for Numerical Methods in Engineering*, **24**, (1987), pp. 359–373. https://doi.org/10.1002/nme.1620240207.

APPENDIX A.

Here, the derivative of the mapping function $\phi_{i,e}$ with respect to the original design variables $x_e^{(j)}$, $\dfrac{\partial \phi_{i,e}}{\partial x_e^{(j)}}$, is presented. Without loss of generality, the authors assume a three-phase example for the following discussion.

Using the chain rule, the derivative $\dfrac{\partial \phi_{i,e}}{\partial x_e^{(j)}}$ is obtained by

$$\frac{\partial \phi_{i,e}}{\partial x_e^{(j)}} = \frac{\partial \phi_{i,e}}{\partial \hat{x}_e^{(j)}} \cdot \frac{\partial \hat{x}_e^{(j)}}{\partial \tilde{x}_e^{(j)}} \cdot \frac{\partial \tilde{x}_e^{(j)}}{\partial x_e^{(j)}}. \tag{A.1}$$

From the definition of the partition-of-unity mapping functions in Eqs. (4)–(6), the derivative $\dfrac{\partial \phi_{i,e}}{\partial \hat{x}_e^{(j)}}$ is calculated by

$$\text{if } i \equiv j: \quad \frac{\partial \phi_{i,e}}{\partial \hat{x}_e^{(j)}} = \frac{\left(\hat{x}_e^{(1)} + \hat{x}_e^{(2)} + \hat{x}_e^{(3)}\right) - \hat{x}_e^{(i)}}{\left(\hat{x}_e^{(1)} + \hat{x}_e^{(2)} + \hat{x}_e^{(3)}\right)^2}, \tag{A.2}$$

$$\text{if } i \neq j: \quad \frac{\partial \phi_{i,e}}{\partial \hat{x}_e^{(j)}} = -\frac{\hat{x}_e^{(i)}}{\left(\hat{x}_e^{(1)} + \hat{x}_e^{(2)} + \hat{x}_e^{(3)}\right)^2}. \tag{A.3}$$

The derivatives $\dfrac{\partial \hat{x}_e^{(j)}}{\partial \tilde{x}_e^{(j)}}$ and $\dfrac{\partial \tilde{x}_e^{(j)}}{\partial x_e^{(j)}}$ are computed based on the definition of projection in Eq. (2) and Eq. (1), respectively. The details have been thoroughly presented in the literature, e.g., see [16, 18], and therefore, will not be repeated here.